CSEM borehole: numerical simulations and experimental tests

Author: Álvaro Cárceles Sánchez
*Facultat de Física, Universitat de Barcelona, Diagonal 645, 08028 Barcelona, Spain.**

Advisor: Pilar Queralt Capdevila

Abstract: The Controlled-Source Electromagnetic (CSEM) method is a geophysical active technique used to investigate subsurface structures and properties of the Earth. In this work I present a numerical simulations of two borehole in Camp dels Ninots (La Selva- Girona) to study CSEM borehole-surface responses. Moreover, I perform an experimental test. The results show that the simulations are too simple, however they show the possibilities of CSEM borehole as high sensitivity and data quality are achieved.

I. INTRODUCTION

Geophysical exploration techniques play a crucial role in our understanding of the Earth's subsurface and provide valuable insights into its geological structures and properties. The CSEM technique is an active method that consists in transmitting electromagnetic waves into the Earth's subsurface using a controlled source. These electromagnetic waves propagate through the incident medium, and their behaviour is influenced by the resistivity distribution. [1] These modified waves arrive to different receivers, and this data can be interpreted to obtain a resistivity profile of the area. This method is commonly used in marine exploration due to high conductivities of oceanic mediums. In this study I will use this method to characterize the subsoil.

Camp dels Ninots, our study area, is located in Caldes de Malavella (Girona, Spain) and belongs to the Catalan Volcanic Zone. The volcan that was in this region was composed of two different substrates, Paleozoic granites and pre-volcanic Pliocene sediments [2]. It has been proven that Camp Dels Ninots is one of the most important archaeological locations in Spain.

To study this region a campaign was performed in 2015, drilling two boreholes CP1 and CP2 with the posterior sounding. The first of the boreholes reaches a depth of 113m and the second one 145m [2]. The CSEM method has never been used in this area.

II. FUNDAMENTALS

A. CSEM theory

The Maxwell's equations are a set of four fundamental equations of electromagnetism [3]. These equations describe completely all the electromagnetism phenomena and are the theoretical basis of the CSEM method:

$$\vec{\nabla} \cdot \vec{D} = \rho, \quad (1)$$
$$\vec{\nabla} \cdot \vec{B} = 0, \quad (2)$$
$$\vec{\nabla} \times \vec{E} = -\frac{\partial \vec{B}}{\partial t}, \quad (3)$$
$$\vec{\nabla} \times \vec{H} = \vec{j} + \frac{\partial \vec{D}}{\partial t}, \quad (4)$$

where t is time (s), $\vec{D}$ is the displacement vector (C/m^2), $\vec{E}$ is the electric field (V/m), $\vec{B}$ is the magnetic B-field (T), $\vec{H}$ is the magnetic H-field (A/m), ρ is the charge density (C/m^3), $\vec{j}$ is the current density (A/m^2) and $\vec{\nabla}$ is the nabla operator. Equation (1) is Gauss's Law for electric field, equation (2) is Faraday's Law, equation (3) is Gauss's Law for magnetic field and equation (4) is Ampère-Maxwell's Law. Other equations that are going to be necessary are the boundary conditions between two mediums for the electric and magnetic field:

$$\vec{n} \cdot \left(\overrightarrow{D_+} - \overrightarrow{D_-}\right) = \sigma, \qquad \vec{n} \times \left(\overrightarrow{E_+} - \overrightarrow{E_-}\right) = 0, \quad (5)$$
$$\vec{n} \cdot \left(\overrightarrow{B_+} - \overrightarrow{B_-}\right) = 0, \qquad \vec{n} \times \left(\overrightarrow{H_+} - \overrightarrow{H_-}\right) = 0, \quad (6)$$

where σ is the electrical conductivity ($\Omega^{-1}\cdot m^{-1}$), $\vec{n}$ is the perpendicular vector between the two mediums and the suffixes '+' and '−' reference each one of the two mediums.

If the medium is homogeneous and isotropic these relations can be established:

$$\vec{D} = \varepsilon \vec{E}, \qquad \vec{B} = \mu \vec{H}, \qquad \vec{j} = \sigma \vec{E}, \quad (7)$$

where ε is the electric permittivity (F/m) and μ is the magnetic permeability (T·m/A). To obtain boundary conditions simplified in homogeneous and isotropic mediums eq. (7) must be replaced in eqs. (5) and (6):

$$\vec{n} \cdot \left(\varepsilon_+ \overrightarrow{E_+} - \varepsilon_- \overrightarrow{E_-}\right) = \sigma, \quad \vec{n} \times \left(\overrightarrow{E_+} - \overrightarrow{E_-}\right) = 0, \quad (8)$$
$$\vec{n} \cdot \left(\overrightarrow{B_+} - \overrightarrow{B_-}\right) = 0, \quad \vec{n} \times \left(\overrightarrow{B_+}/\mu_+ - \overrightarrow{B_-}/\mu_-\right) = 0. \quad (9)$$

In the CSEM method a transmitter is used which implies that an additional term for the current density must be added:

$$\vec{j} = \sigma \vec{E} + \overrightarrow{j_t}, \quad (10)$$

where $\overrightarrow{j_t}$ is the transmitter current density (A/m^2). Replacing eqs. (7) and (10) in eqs. (1) and (4) and assuming harmonic electric and magnetic fields:

$$\vec{\nabla} \times \vec{E} = i\mu\omega \vec{H}, \quad (11)$$
$$\vec{\nabla} \times \vec{H} = \overrightarrow{j_t} + (\sigma - i\varepsilon\omega)\vec{E}, \quad (12)$$

where ω is the angular frequency of the magnetic and electric fields (s^{-1}). Most of the materials are not magnetic materials which it involves that their permeability is equal to the permeability of free space μ_0. The CSEM method use low

frequencies (0.125-32Hz in my case) which involves that $\sigma >> \varepsilon\omega$ and we can simplify eq. (12):

$$\vec{\nabla} \times \vec{H} = \vec{J_t} + \sigma\vec{E}. \quad (13)$$

B. Forward modelling

In applied geophysics two fundamental operating modes can be distinguished. These two modes are the forward model and the inverse model.

The forward model, in our case, consists in the numerical simulation of the expected electromagnetic response of the subsurface based on a given resistivity distribution. It involves solving Maxwell's equations and simulating the propagation of electromagnetic waves through the subsurface. The forward model allows us to estimate the parameters such as the geometry of the survey, the properties of the source, and the receiver configuration. To use this model, a priori information on the resistivity distribution of the studied area is needed, what at first is unknown.

C. Inverse modelling

The inversion model in CSEM refers to the process of determining a resistivity profile of the subsurface starting from the measured electromagnetic data. This inversion process is performed by an iterative algorithm with the objective to minimize a certain target misfit respect the forward model. Inversions have been done previously to collect the experimental data with the objective to test if we will have sensitivity to a priory model.

III. SIMULATIONS

One interesting thing to do before realising the experimental setup in Camp dels Ninots is to simulate the resistivity map of the two boreholes CP1 and CP2. I will use Kerry Key's software OCCAM1DCSEM [3]. This software can do both the forward and inverse model for a 1D model, where the resistivity changes only on depth.

As initial model of the resistivity profile I use the models obtained from [2]. The models are presented as discrete layers with three layers in the case of CP1 and four layers in the case of CP2. In the case of CP2, the depth at which the deepest layer begins is not well defined.

Material and resistivy	CP1	CP2
Sediments (10 Ω·m)	0-65m	0-63.2m
Tuff (50 Ω·m)	65 - 103.8m	63.2-115.2m
Paleozoic granite (1000 Ω·m)	103.8-130m	-
Pyroclasts / Basalt (200/1000 Ω·m)	-	115.2-145m

Table I: Theoretical geological composition of CP1 and CP2.

To start the simulation, I start to run the program from arbitrary values for the electrical fields obtained in each receiver but with the model corresponding to the boreholes (see Table 1). The forward responses of OCCAM1DCSEM are the theoretical data as well as the expected ones.

With this new data obtained by the forward model, I can replace the arbitrary fields, give them an error, and run the inversion model. This inversion process will return a resistivity profile similar to the initial modelling with a smoother variation with depth. In the simulation case, the field is going to be emitted from ten different depths (ten transmitters) inside the borehole from 0.5m to 80m. This field is going to be registered by five receivers located in the same straight line from 5m to 75m. Since the receivers are located on a single axis, I am only going to measure the field on that axis because is much larger than in the others. I will consider an error of 10% for the data and different frequencies between 0.8Hz to 5Hz. Considering all this the simulation can be started. With these parameters, the model for CP1 converges with 5 iterations while the model CP2 doesn't converge. The criteria used for the convergency is that the root mean square (RMS) is equal to unity. To make the model converge the error I incremented the error considered in the data, but precision decrease.

Figures 1a and 1b show the amplitude of the electric field decays linearly with the distance to the borehole. The deeper the transmitter is respecting the borehole the less amplitude received (T1 refers to the most superficial transmitter and T10 refers the deepest one). In these graphs the amplitudes of the electric field are only represented for one frequency (0.8Hz), this is because the graphs obtained with the rest of the frequencies were practically identical. One thing to highlight is that the response obtained by the forward model is almost the same in both boreholes, this is because, the first two layers are identical, and these occupy most of both boreholes. The only changes are due to the deeper layers. These changes are practically insignificant and represent a minimum change in the amplitude measured at the most distant receivers.

Figures 2a and 2b show a smooth and continuous resistivity profile is obtained. These models coincide almost perfectly with the theoretical model in the first layer, but they lose precision as we increase the depth. The region where they present worse precision is in the deepest layer, in which the initial model cannot be recovered. In the intermediate layers a continuous model that fits the initial discrete model quite precisely is obtained.

To solve this precision error in the deepest layer I fix it to the expected value given by the theoretical model. Figure 3 shows the deepest layer coincides perfectly, but all the model changed, losing precision in the intermediate layers, and not recovering the initial model.

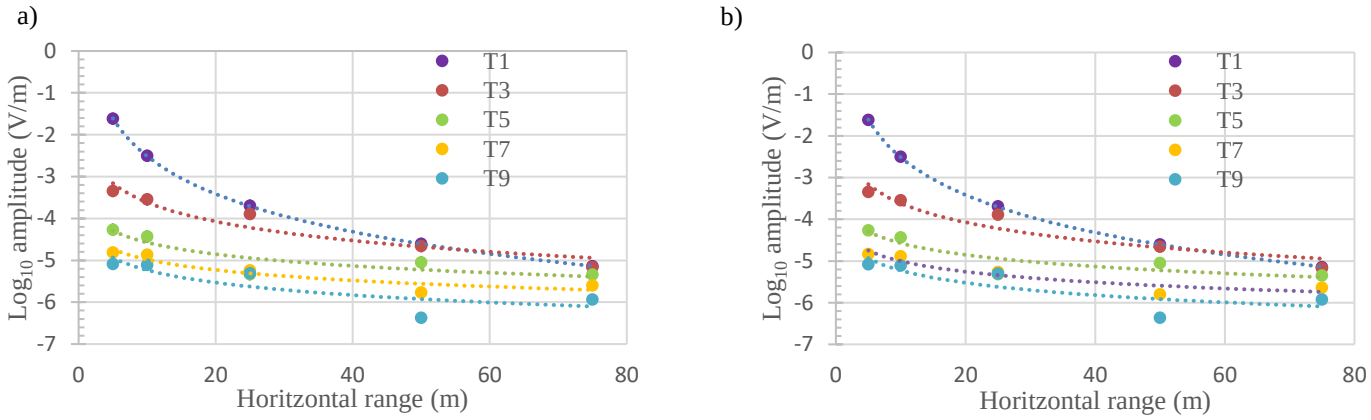

Figure 1: Electric field obtained from the forward modelling at each receiver correspondent to each transmitter for CP1 (a) and CP2 (b) with the corresponding logarithmic trendlines obtained with Excel.

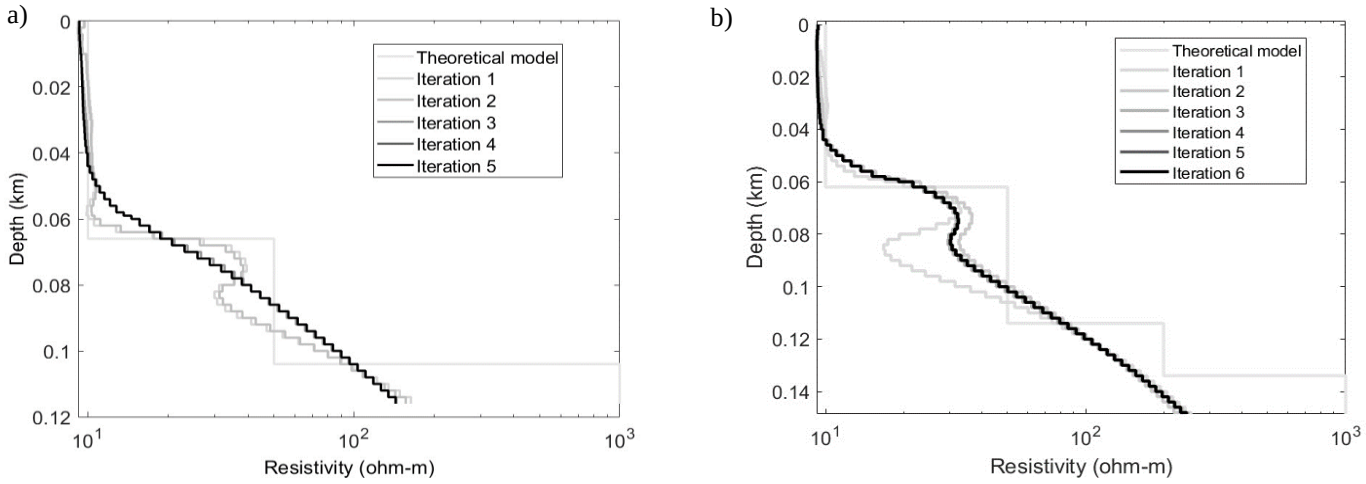

Figure 2: Resistivity profile obtained from the inverse modelling for CP1 with an error of 10% (a) and for CP2 with an error of 20% (b).

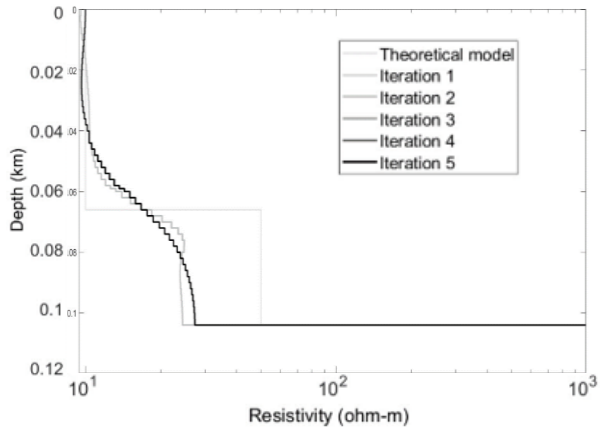

Figure 3: Resistivity profile obtained from the inverse modelling for CP1 with an error of 10% with the deepest layer fixed.

IV. EXPERIMENTAL SETUP

A. First day

The first test was performed on 17th May. The equipment consisted of a ZT-30 transmitter connected to a set of car and truck batteries in series. This transmitter can operate on time-domain signal between 0 (DC) and 32Hz or on a frequency between 0 (DC) and 512Hz. The output transmitter was connected to a pair of electrodes introduced inside CP1 with the idea to do the emission at different depths.

To control the frequency of the transmitter we used an XMT-G transmitter controller. This device was necessary to create a square signal of a precise frequency. In my case I used signals between 0.125Hz and 8Hz. A sampling frequency of 500Hz and gains 1 were used for both days.

To receive the signal, I used a set of 5 SRU Spider data loggers. These data loggers were connected to a GPS and to a

car or motorcycle battery. They were also connected to a pair of electrodes in each direction of the data logger. These electrodes were connected every 10 meters and they were oriented 43° in S-W direction (fig.4).

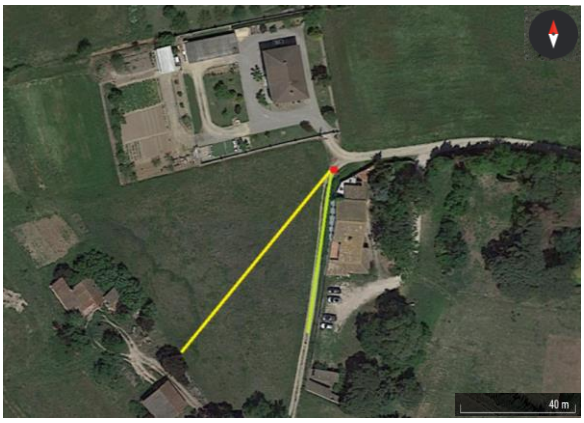

Figure 4: Satellite map of Camp del Ninots from Google Earth with the location of CP1(red dot), first day electrode orientation (yellow line) and second day electrode orientation (green line).

Before starting the experimental setup the level of water in the borehole where measured with a probe resulting 24.15m.

The transmitter ZT-30 did not work properly, and after several failed trials, the experiment must finish, hopping to have another opportunity once in the laboratory solve the technical problem.

B. Second day

The 7th June, a new test were performed in the same place. The experimental configuration was optimized: instead of placing the receivers through the field, we placed them along the path (fig. 4)

First configuration: Borehole-surface

Firstly, the receivers (Rx) were placed on the path where CP1 is located. These receivers consisted of two electrodes separated 20m and a datalogger spider placed between both. A receiver Rx was placed about 5m away (spider n.65) and a second receiver Rx 20m away from the first receiver (spider n.67). The spider (n.69) was next to the borehole and connected to the ZT-30 transmitter that gave us the signal injected to CP1 (Tx). This signal was injected by two steel electrodes separated by about 35 cm and designed to be in boreholes, these were placed at a depth of 40m (assuring that they were already in the water considering that it was at a height of about 25m). A first test was done with this configuration.

When performing this test with a square signal of 2Hz from the transmitter, the emitted signal was received correctly with the spider n.69 (Tx), but this signal was practically imperceptible in the other two spiders (Rx). To increment the received signal the first receiver was approached to the borehole, but the upgrade was insignificant.

A weak current (0.2A) was inserted with 8 batteries of 12V. A very high contact resistance (18KΩ) was observed between the borehole electrodes.

Second configuration: Surface-borehole

To be able to solve this problem the experimental setup was changed to the "surface-borehole" configuration, now the electrodes located inside the borehole act as a receiver instead as a source. As an emitter 2 large electrodes were used at a distance from the borehole of 15m the first and 45m the second, therefore the center of the emitter was at 30m from the borehole. A casing was done with PVC to hold the electrodes. To reduce the contact resistance bentonite was applied around the electrodes. The spider n.69 continued monitoring the inserted current while the spider n.67 monitored the electrodes inside the borehole. Again, a first test was done with a 2Hz square signal, and in this case, we were able to detect the square signal inside CP1 (in this case the injected current was 0.7A acquired with 9 batteries of 12V). This emission was repeated for different frequencies with different times for each one. To increase the conductivity of the subsurface we applied bentonite at the electrodes of the transmitter.

V. RESULTS

Figure 5a shows the spectrogram of spider n.67 located at the farthest receiver in the first configuration and associated with the borehole's receivers in the second configuration. The first thing to highlight in the spectrogram is the abrupt change (at 8000s) of signal amplitude, this instant corresponds to the instant we changed the configuration. The spider n.67 went from recording the signal from the electrodes on the surface (borehole-surface configuration) to recording the signal from the electrodes in the borehole (surface-borehole configuration).

A peak of amplitude is observed in the frequency corresponding to 50Hz, that is because this is the frequency of the electricity network. Smaller intensity peaks can be appreciated corresponding to the higher harmonics of this frequency. However, the most interesting region of the spectrogram can be seen close to 50Hz once the configuration of the electrodes has been changed. Zooming in on that specific area Figure 5b is obtained.

This region shows the peaks at the frequencies at which we emitted, as well as their corresponding higher odd harmonics (because the emitted signal is square), so that verifies that the signal arrives correctly.

The processing data were made using the code from Vilamajó [1]. Figure 5c presents the transfer function of data recorded on the electrodes inside the borehole.

In the case of the amplitude, it represents a dependence of the frequency, contrary to what is seen with the simulations. For the phase, on the other hand, the variation is much smaller with frequency. Figure 6 shows the inverse model obtained with the real data fixing the deepest layers so that the model converges.

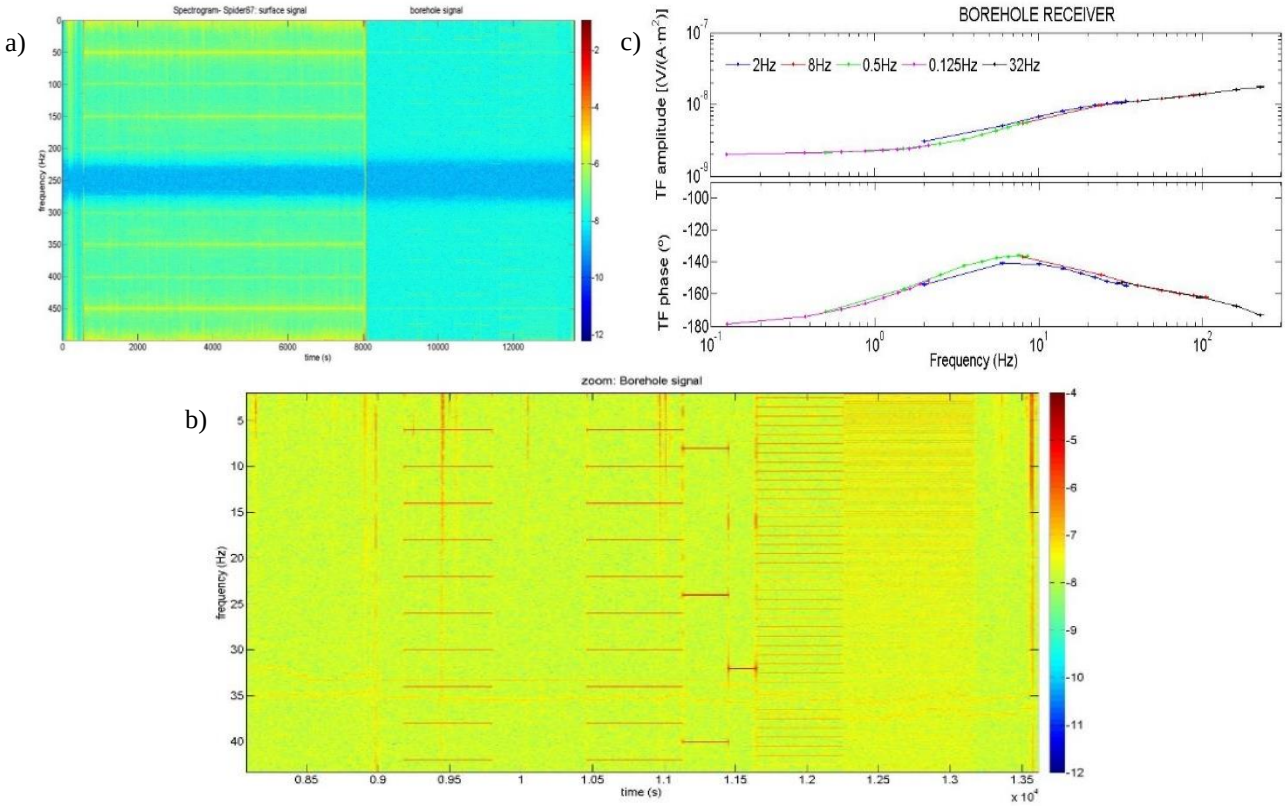

Figure 5**.** Spectrogram corresponding to the data captured by the spider n.67 (a), zoom corresponding to the data captured by the spider n.67 after changing the configuration (b), amplitude and phase of the transfer function of our montage (c).

A very high conductivity is observed in the first layers, possibly due to the effect of the bentonite and a very high resistivity at deeper levels corresponding to the effect of PVC.

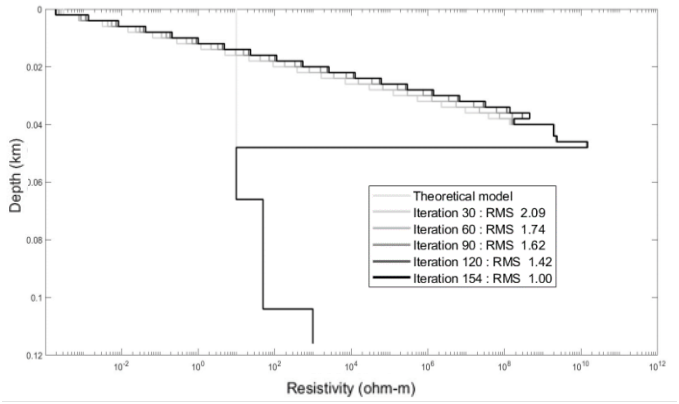

Figure 6**.** Resistivity profile obtained from the inverse modelling for the real data measured at CP1.

VI. CONCLUSIONS

On this project, I have shown how simulations can give us a first idea of what the subsoil is like, but they are unable to recover the theoretical model. I have also demonstrated the variety of these by fixing specific layers and how they do not fit the experimental data.

As well, I have been able to see that emissions show much greater efficiency when performed in the configuration surface-borehole and the data show the effect of the formation near the hole, including the bentonite and the PVC.

The simulations were made considering 1D models. A next step of this research could be use a 3D code in order to include the effect of the plastic casing as well as the water inside.

Acknowledgements

I would like to specially thank my advisor Pilar Queralt for her invaluable help, support and patience. I also want to thank my mother Maria Fuensanta Sánchez and my closest friend Carmen Torruella for all their support.

[1] E. Vilamajó, «CSEM monitoring at the Hontomín CO_2 storage site: modeling, experimental design and baseline results.»

[2] Institut Cartogràfic i Geològic de Catalunya, «Campanya de prova amb mètodes geofísics al Camp dels Ninots »

[3] E. Mills and D. J. Morin, «Electricity and Magnetism»

[4] K. Key, «1D inversion of multicomponent, multifrequency marine CSEM data: Methodology and synthetic studies for resolving thin resistive layers».